Supporting Information

Datta et al. 10.1073/pnas.1217517110

SI Text

SI Materials and Methods

Data Analysis. Velocities were estimated using the following procedure:

1. Profiles were fit to hyperbolic tangents. The spatial wave profiles from individual days were fit to the function indicated in *Analytical Results Regarding Population Density Waves*. All fits were performed with MATLAB version R2012a nlinfit from the Statistics Toolbox. We chose to fit individual profiles from each day, rather than forcing a single set of parameters to fit all profiles simultaneously. The choice was made to account for the slight day-to-day variation in the bulk density and wave profile shape that we observe experimentally. We note that, for the genetic waves shown in Fig. 4, we approximated the shape of the wave profile with the same functional form that was used for the population waves. However, this fit is not theoretically predicted.
2. The plot of midpoint position X_m vs. time was fit to a line. From the fits of the wave profiles, we inferred a midpoint position (X_m) for each day. The trajectory of the midpoints over time was fit to a line, and the velocity of the wave was estimated from the slope. Linear fits were performed with MATLAB version R2012a function polyfit.

Estimation of Error and Statistical Significance. Errors for velocity measurements (v_{coop}, $v_{invasion}$, and v_{mixed}) were estimated from a single, 9-d run of the experiment based upon the SE in the slope of the X_m vs. time regression line (1). We note that each day of the experiment can be viewed as an internal technical replicate in which the midpoint of the wave (X_m) is measured in an identical fashion. Because the velocities are the slopes of the X_m vs. time regression line, the high quality of these fits reflects the consistency of the technical replicates. Consequently, the error bars that we have reported (SEs of the slope of the regression line) reflect our confidence in the velocity measured in that particular experiment.

To estimate the significance of differences between v_{coop} and $v_{invasion}$ at a particular dilution factor, we fit the combined X_m data used to obtain both velocities to a linear regression model. This model contains an interaction between two predictors (time and a dummy variable for the cooperators) represented as differential slope (v_{diff}) and intercept (β_1) terms (see below):

$$X_m = \beta_0 + \beta_1(\text{cooperator}) + v_{invasion}(\text{time}) + v_{diff}(\text{time})(\text{cooperator}).$$

We performed a standard two-tailed t test to obtain a P value for v_{diff}, which provides a direct estimate of the probability of seeing the measured difference between v_{coop} and $v_{invasion}$ purely by chance (2, 3).

Numerical Simulations in a Discrete Linear Stepping-Stone Model with Realistic Well Dynamics. To gain intuition for our experimental system, we performed numerical simulations using a model that well approximates the experiments that we performed. Here, we summarize the formulation of this model, and we demonstrate that the model features are sufficient to predict our main experimental results.

Modeling individual well dynamics in the absence of spatial coupling. To model the cooperative dynamics within experimental yeast populations, we used a previously developed growth model based upon experimental measurements. This model has been discussed extensively in the supplementary information of (4) and (5). Briefly, previous work has shown that, owing to the cooperative nature of growth in sucrose medium, the exponential growth rates of both cooperators and defectors change as a function of the cell density. Under low-density conditions, the growth rate of the cooperators is higher than that of the defectors ($\gamma_{C_{low}} > \gamma_{D_{low}}$), because the defectors are unable to take advantage of the glucose produced by cooperators in the environment and cooperators retain some preferential access to the glucose that they produce. This trend is reversed at high cell densities ($\gamma_{C_{high}} > \gamma_{D_{high}}$) because defectors can consume the glucose produced by cooperator cells without having to pay the "cost" of cooperation (4).

A schematic of this two-phase growth model is illustrated in Fig. S5*A*. Because each well is well-mixed and nutrient-limited, yeast growth is modeled to be logistic with a carrying capacity ($K \approx 10^8$cells/mL), with low- and high-density phases delineated by a critical cell density, ($N_{critical} \approx 3 \times 10^5$cells/mL). Given that $N_{critical}$ is over two orders of magnitude lower than K, we assumed that $\gamma_{C_{low}}$ and $\gamma_{D_{low}}$ was approximately constant (no logistic decline). However, above $N_{critical}$, the growth rates were assumed to decrease from maximum values ($\gamma_{C_{high}}$ and $\gamma_{D_{high}}$) according to the logistic equation.

For all simulations, the growth rates were chosen in accordance with previous experimental measurements (4) as follows: $\gamma_{C_{low}} = 0.33\ \text{h}^{-1}$, $\gamma_{C_{high}} = 0.45\ \text{h}^{-1}$, $\gamma_{D_{low}} = 0.31\ \text{h}^{-1}$, and $\gamma_{D_{high}} = 0.46\ \text{h}^{-1}$.

Formulation of discrete linear stepping-stone model. As in the experiments, the simulations involve a population of cells that is separated among several discrete, well-mixed subpopulations arranged on a line. Initially, a certain number of wells is populated with cells, whereas the remainder are unpopulated to allow for expansion of the population into new territory. After 23 h of simulated growth, a portion of the cells ($\frac{m}{2} = 0.25$, as in the experiments) is transferred into each of the neighboring wells. The entire population is then decreased in size by a fixed factor, which represents a death process in the growth dynamics. Simulations typically involve 10 repetitions of this cycle. Midpoints of wave trajectories (X_m) and wave velocities were estimated using the procedure described in *Materials and Methods*.

Features of this model are sufficient to recapitulate our experimental results. Fig. S5 *B* and *C* show simulations of the model (using the parameter values shown above). As indicated in the figure, the features of this simple phenomenological model are sufficient to recapitulate the qualitative results observed experimentally. Fig. S5*B* indicates that, as demonstrated experimentally, the cooperator allele is favored at the front of the expanding populations. Fig. S5*C* illustrates the simulated relationship between the cooperator velocity v_{coop} and the invasion velocity $v_{invasion}$ over a range of dilution factors. As we demonstrated experimentally, the model predicts that $v_{coop} > v_{invasion}$ at low dilution factors, but that $v_{coop} < v_{invasion}$ at high dilution factors.

Analytical Results Regarding Population Density Waves. Although empirical studies of expanding populations are few and far between, the ecological theory of range expansions has a long history. Reaction–diffusion models are widely used in physics (6, 7), chemistry (8), and biology (9). Spatial models of range expansions based upon reaction–diffusion equations were first discussed by Fisher (10) and Kolmogorov (11) in the late 1930s, and a good summary of the results is found in ref. 12.

Surprisingly, the wave front profiles that we observed empirically were well approximated by these continuous-time,

continuous-space models, even though our experiments were discrete in time and space. Here, we summarize the formulation of a model of range expansions and some useful results. In accordance with our experiments, we only discuss one-dimensional expansions here.

The dynamics of range expansions are dictated by both the growth of the population and the dispersal of individuals into unpopulated territory. For short-range, isotropic dispersal, the process can be modeled with a diffusion term. Thus, the model can be formulated as the reaction–diffusion equation shown below:

$$\frac{\partial c}{\partial t} = D\frac{\partial^2 c}{\partial x^2} + G_c(c)c, \qquad [1]$$

where $c(x,t)$ is the population density at position x and time t, D is the effective diffusion coefficient for population dispersal, and G_c is the per capita growth rate of the population. Note that $D = \frac{m}{2}$, where $\frac{m}{2}$ is the portion of cells transferred into each of the neighboring wells in the discrete simulations.

In principle, $G_c(c)$ could be any one of a number of functions, depending upon the growth dynamics of the specific population in question. In our cooperatively growing yeast populations, we found that $G_c(c)$ depends nonmonotonically on the population density $(c(x,t))$ (5). In general, a habitat has a carrying capacity K owing to resource limitation, and populations usually grow at a reduced or negative rate close to this upper bound on the density. Populations displaying cooperative behaviors also tend to grow slowly or not at all at low densities, because interactions between individuals are limited. Thus, unlike the standard logistic model, the per capita growth rate is maximized at an intermediate population density. This nonmonotonic dependence of the per capita growth rate on the population density is known as the Allee effect (5, 12, 13). The most common model of growth with an Allee effect assumes the following form for the per capita growth rate:

$$G_c(c) = g_c(K-c)\left(c-c^*\right), \qquad [2]$$

where K is the carrying capacity, c^* is the critical population density, and g_c modulates the overall magnitude of the per capita growth rate (12, 13). The strong Allee effect describes the case in which $c^* > 0$, whereas a weak Allee effect occurs when $-\frac{K}{2} < c^* < 0$ (13).

This reaction–diffusion equation admits traveling wave solutions with a time-invariant density profile that moves at a constant velocity. Although nonlinear partial differential equations of this type are often difficult to solve analytically, exact solutions for the velocity and shape of the wave profile are known exactly. The expression for the velocity is shown below:

$$v = \begin{cases} \sqrt{\frac{Dg_c}{2}\left(K-2c^*\right)}, & \text{if } c^* \geq -\frac{K}{2} \\ 2\sqrt{Dg_cK|c^*|}, & \text{if } c^* < -\frac{K}{2} \end{cases}. \qquad [3]$$

Previous work has shown that our experimental system demonstrates a strong Allee effect $(c^* > 0)$ and that K and c^* approach each other with increasing dilution factor (5). Thus, the analytical expression shown above predicts that the traveling wave velocity should decrease with increasing dilution factor, in line with what we observed experimentally (Fig. 5*A*).

The shape of the time-invariant wave profile is given by

$$c(\xi) = \frac{\mathrm{K}}{1+e^{\sqrt{\frac{g_c}{2D}}\mathrm{K}\xi}} = \frac{\mathrm{K}}{2}\left[1-\tanh\frac{1}{2}\sqrt{\frac{g_c}{2D}}\mathrm{K}\xi\right]$$
$$= \frac{\rho_{\max}}{2}\left[1-\tanh\left(\frac{x-\mathrm{X_m}}{w}\right)\right], \qquad [4]$$

where $\xi = x - vt$, and we set $K = \rho_{\max}$, $\xi = x - \mathrm{X_m}$, and $w = 2K\sqrt{\frac{2D}{g_c}}$ to connect this analysis to our experimental results.

The population density wave profiles that we observed experimentally were well fit by this functional form. Thus, by fitting profiles from each day to this function, we obtained estimates of $X_m(t)$ and $\rho_{\max}(t)$.

Analytical Results Regarding Genetic Waves. The spreading of cooperator and defector alleles can also be modeled with a reaction–diffusion equation like the one shown below:

$$\frac{\partial f}{\partial t} = D\frac{\partial^2 f}{\partial x^2} + G_f(f)f, \qquad [5]$$

where $f(x,t)$ is the frequency of the defector allele at position x and time t, D is the effective diffusion coefficient for population dispersal, and G_f is the relative growth rate of defectors, which is a function of f to model frequency-dependent dynamics.

Frequency-dependent selection is most often modeled with the following function:

$$G_f(f) = g_f(1-f)\left(f^*-f\right), \qquad [6]$$

where $g_f \geq 0$ is the strength of selection and f^* is the equilibrium frequency of defectors in a well-mixed population.

Using this model and the results from ref. 11, the velocity of defectors invading a spatially extended population of cooperators can be shown to be

$$\mathrm{v_{invasion}} = 2\sqrt{Dg_ff^*}. \qquad [7]$$

As shown in Fig. S5, the equilibrium frequency of defectors decreases with increasing dilution factor. Thus, if g_f remains constant, the above result predicts that $v_{invasion}$ should decrease monotonically with the dilution factor.

Discussion of Outrunning. In the main text, we suggest that a "sufficiently large" leading region of cooperators is required for outrunning to occur. To develop this idea further, we can consider the relative movement of the invasion wave (consisting of a mixture of cooperators and defectors in our experiments) and the pure cooperator wave, both of which have finite widths because organisms are discrete entities (14). If the separation between the two waves is such that the invasion wave front ends before the cooperator wave front begins, then outrunning will occur if and only if $v_{coop} > v_{invasion}$.

Interestingly, the notion of outrunning could be extended to a wide range of systems outside of the case in which cooperators outrun an invading wave of defectors. A particular example with frequency-dependent selection is considered in the supplementary appendix of ref. 15.

1. Freedman D, Pisani R, Purves R (2007) *Statistics* (W.W. Norton, New York).
2. Devore JL, Farnum NR (2004) *Applied Statistics for Engineers and Scientists* (Duxbury Press, Belmont, CA), 2nd Ed.
3. Peck R, Devore JL (2011) *Statistics: The Exploration & Analysis of Data* (Brooks/Cole, St. Paul, MN), 7th Ed.
4. Celiker H, Gore J (2012) Competition between species can stabilize public-goods cooperation within a species. *Mol Syst Biol* 8:621.
5. Dai L, Vorselen D, Korolev KS, Gore J (2012) Generic indicators for loss of resilience before a tipping point leading to population collapse. *Science* 336(6085):1175–1177.

6. Kerner BS, Osipov VV (1994) *Autosolitons: A New Approach to Problems of Self-Organization and Turbulence* (Springer, Berlin).
7. Scholl E (2001) *Nonlinear Spatio-Temporal Dynamics and Chaos in Semiconductors* (Cambridge Univ Press, Cambridge, UK).
8. Grzybowski B (2009) *Chemistry in Motion: Reaction-Diffusion Systems for Micro- and Nanotechnology* (Wiley, New York).
9. Britton NF (1986) *Reaction-Diffusion Equations and Their Applications to Biology* (Academic, New York).
10. Fisher RA (1937) The wave of advance of advantageous genes. *Ann Eugen* 7:355–369.
11. Kolmogorov A, Petrovskii I, Piscunov N (1937) A study of the equation of diffusion with increase in the quantity of matter, and its application to a biological problem. *Byul Moskovskogo Gos Univ* 1:1–25.
12. Murray JD (2003) *Mathematical Biology II* (Springer, Berlin), 3rd Ed.
13. Courchamp F, Clutton-Brock T, Grenfell B (1999) Inverse density dependence and the Allee effect. *Trends Ecol Evol* 14(10):405–410.
14. Hallatschek O, Korolev KS (2009) Fisher waves in the strong noise limit. *Phys Rev Lett* 103(10):108103.
15. Hallatschek O, Nelson DR (2010) Life at the front of an expanding population. *Evolution* 64(1):193–206.

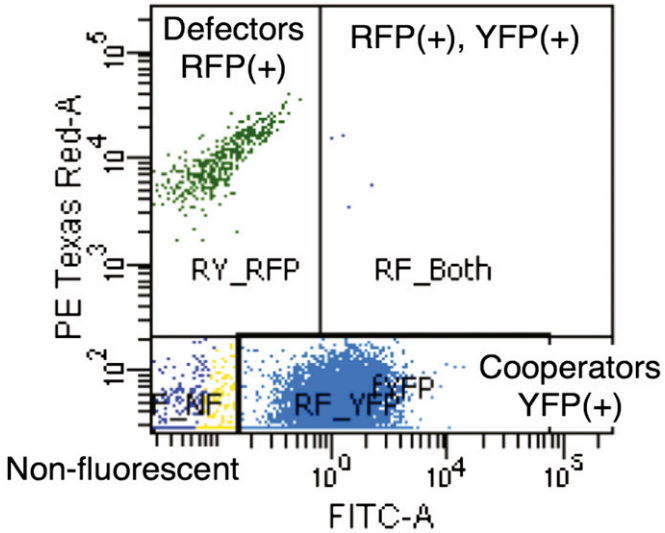

Fig. S1. Distinguishing the two alleles with flow cytometry. The cooperator strain is labeled with yellow fluorescent protein (YFP) that is expressed constitutively from the ADH1 promoter, and the defector strain is labeled with tdTomato expressed constitutively from the PGK1 promoter. We distinguish the two strains with a Becton Dickinson LSR II HTS flow cytometer with an excitation laser at 488 nm. An emission filter at 530/30 nm detects YFP fluorescence, and a filter at 575/26 nm detects red fluorescent protein (RFP) fluorescence. The plot above is from a sample from d 6 of the expansion of a mixed population of cooperators and defectors. The two strains are distinguished based upon RFP fluorescence and separated with the gates shown. This separation identifies 782 defectors out of a total of 17,983 cells, yielding an estimate of \(f = 0.96\) as the frequency of cooperators. A small number of cells (181) were nonfluorescent (gated in the bottom right), and seven counts were deemed both RFP- and YFP-positive, which indicated that multiple cells were detected simultaneously.

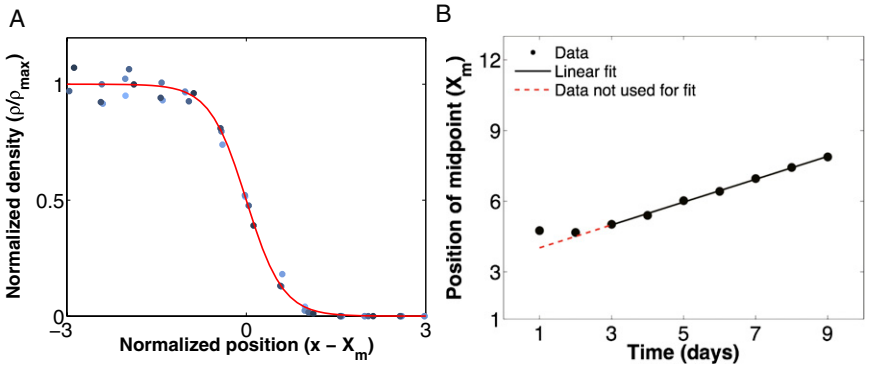

Fig. S2. Mixed cooperator–defector populations expand as traveling waves. (*A*) An overlay of the density profiles from the last 7 d of a one-dimensional expansion of a mixed cooperator–defector population ($m = 0.5$ and dilution factor = 600) at its equilibrium cooperator frequency. Each profile is normalized to the maximum density found in the bulk population (ρ_{max}) and shifted by its midpoint position (X_m). The red line shows a fit to the hyperbolic tangent function derived in *SI Text*. (*B*) Similar to the pure cooperator wave, we can measure the velocity of the mixed cooperator–defector wave by plotting the position of the density profile midpoint (X_m) vs. time and then finding the slope of the line. As in *A*, data from the first 2 d are not included in the fit, because the expanding population has not reached a steady-state density profile.

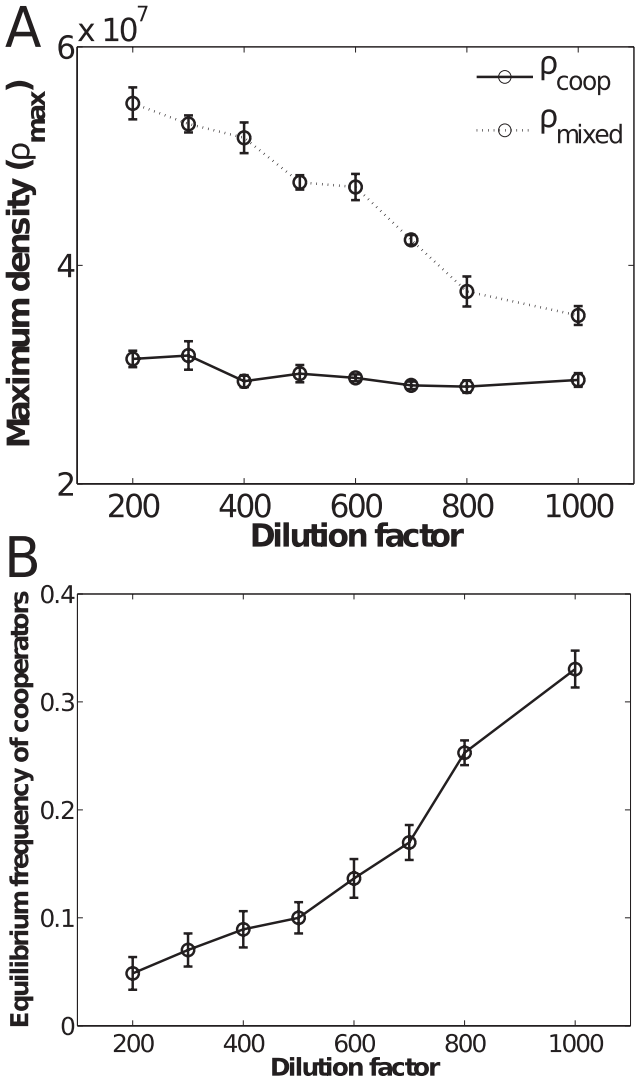

Fig. S3. Effect of dilution factor on the population density in the bulk $(\rho_{\max})$ and equilibrium frequency of cooperators. (*A*) The maximum population density (found in the bulk population) over a range of dilution factors between 200 and 1,000. Values of ρ_{max} were estimated based upon fits of individual density profiles to the hyperbolic tangent function derived in *SIText*. It is important to note that histidine is limited in the growth media (*Materials and Methods*). Because the cooperator strain is a histidine auxotroph (and the defector strain is not), these conditions limit the growth of the cooperator strain without strongly affecting the defector strain. Moreover, it is likely that the mixed populations saturate at a higher density owing to this difference in auxotrophy. Error bars indicate the SEM for measurements with $n = 6$. (*B*) The equilibrium frequency of cooperators that would be reached in a well-mixed population undergoing serial growth and dilution by a fixed dilution factor. Estimates of the equilibrium frequency were obtained by averaging the cooperator frequency in the leftmost two wells (those least affected by expansion dynamics on the front) over the last 5 d of the experiment. Error bars indicate the SEM for measurements with $n = 6$.

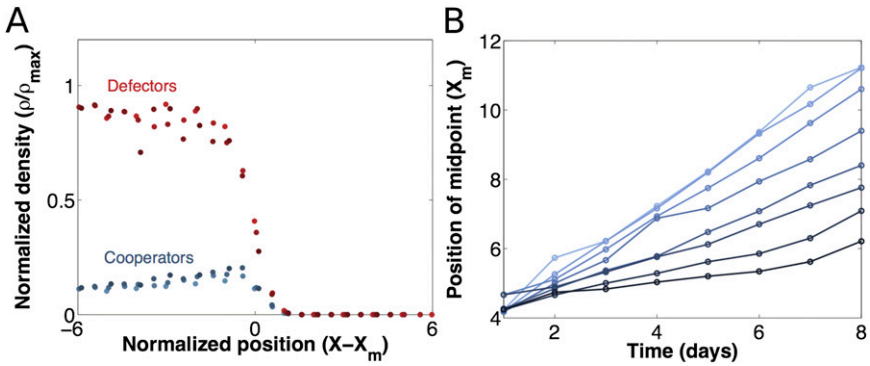

Fig. S4. (*A*) Cooperator density within the mixed cooperator–defector wave peaks near the front of the wave. An overlay of the cooperator and defector population density profiles within the mixed cooperator–defector wave. Data are shown from the last 4 d of the experiment ($m = 0.5$ and dilution factor = 600), where darker circles indicate later time points. Each profile is normalized to the maximum density found in the bulk population (ρ_{max}) and shifted by its midpoint position (X_m). Both cooperators and defectors adopt a time-invariant spatial profile, and the cooperator density peaks at a position near the front of the mixed cooperator–defector wave. (*B*) Velocity of expanding cooperator populations decrease with increasing dilution factor. The midpoint of expanding cooperator waves (X_m) plotted over time for a range of dilution factors between 200 and 1,000 ($m = 0.5$). Darker colors indicate higher dilution factors. All X_m trajectories are roughly linear in time with slopes that decrease monotonically with increasing dilution factors.

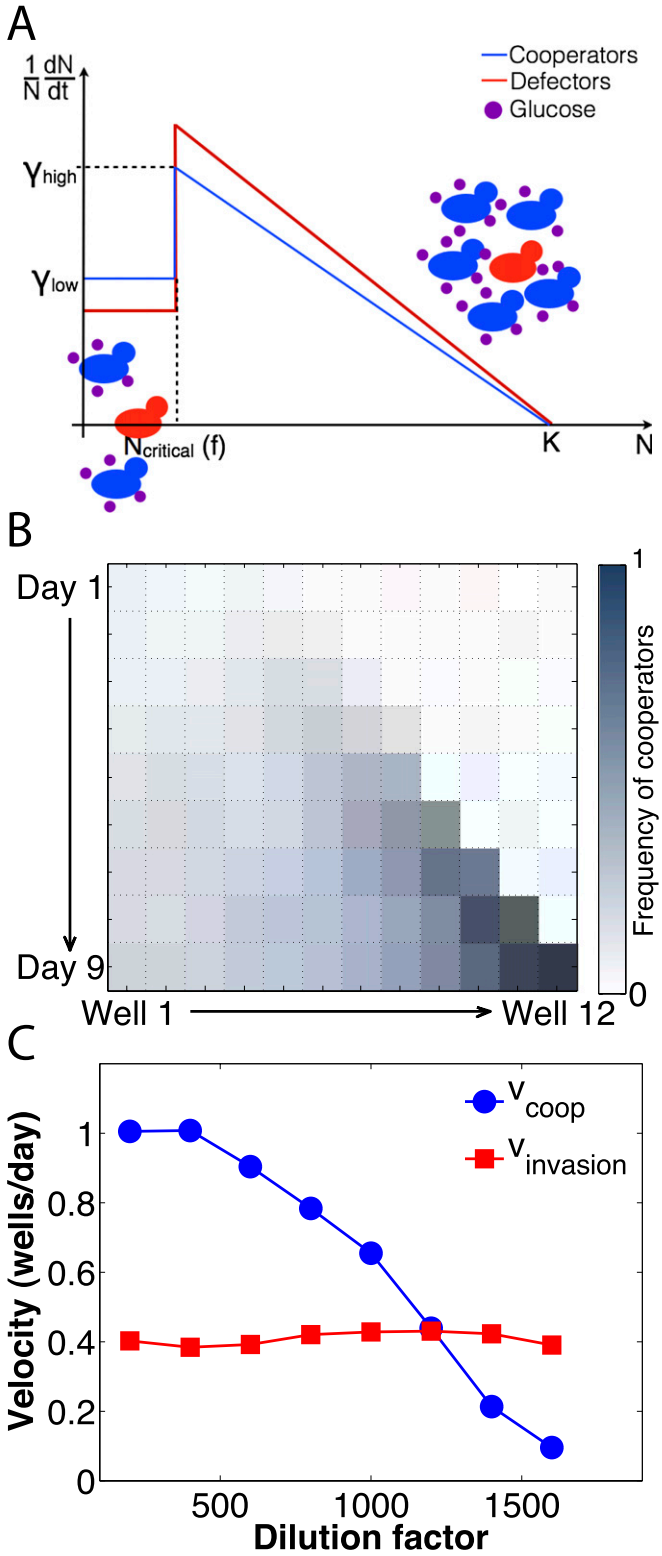

Fig. S5. Formulation of discrete model and simulation results. (*A*) Formulation of the model used to simulate growth dynamics in individual wells in discrete simulations. The schematic depicts the per capita growth rate of cooperators and defectors as a function of cell density. Yeast growth is modeled as logistic with a carrying capacity ($K \approx 10^8$ cells/mL). Low- and high-density growth phases are delineated by a critical cell density, $N_{critical} \approx 3 \times 10^5$ cells/mL. Because $N_{critical}$ is over two orders of magnitude lower than K, $\gamma_{C_{low}}$ and $\gamma_{D_{low}}$ are assumed to be approximately constant (no logistic decline). However, above $N_{critical}$, the growth rates are assumed to decrease from maximum values ($\gamma_{C_{high}}$ and $\gamma_{D_{high}}$) according to the logistic equation. (*B*) Discrete simulation of the frequency of cooperators as a function of time and space. Parameter values are as described in *SI Text*. As we found experimentally, the discrete model predicts that the cooperator allele is enriched at the front of expanding populations. (*C*) Discrete simulation of the velocity of cooperators (v_{coop}) and the velocity of defector invasion ($v_{invasion}$) as a function of dilution factor. Parameter values are as described in *SI Text*. As we demonstrated experimentally, the discrete model predicts two growth regimes, in which $v_{coop} > v_{invasion}$ at low dilution factors and $v_{coop} < v_{invasion}$ at high dilution factors.

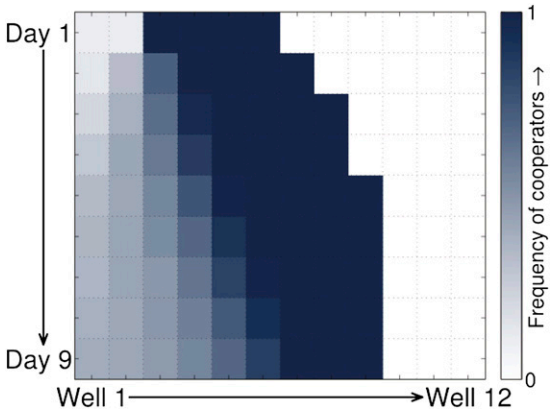

Fig. S6. Cooperators do not outrun defectors at high dilution factors. Experimental observation of defectors invading a spatially extended population ($m = 0.5$ and dilution factor = 800). Under these conditions, $\Delta v = v_{coop} - v_{invasion} \approx -0.1$ wells/d. Over 9 d, the "headstart" region containing pure cooperators decreases from four to three wells, suggesting that the cooperators and defectors will eventually become completely mixed and spread together under these conditions.

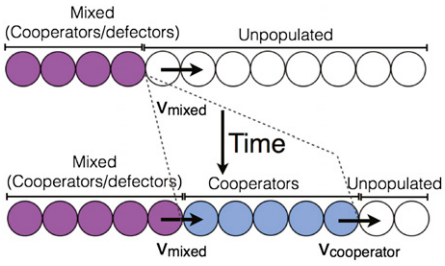

Fig. S7. Schematic of "splitting" in expanding populations. In theory, it is possible for cooperators to split from an expanding mixed population of cooperators and defectors, after which the cooperators travel as a pure wave ahead of the mixed wave. We did not observe this effect experimentally, even under conditions in which (*i*) the cooperator allele was enriched on the front and (*ii*) the cooperators could "outrun" the defectors. Our result is consistent with theoretical predictions suggesting that these two features are necessary but not sufficient conditions for splitting to occur.

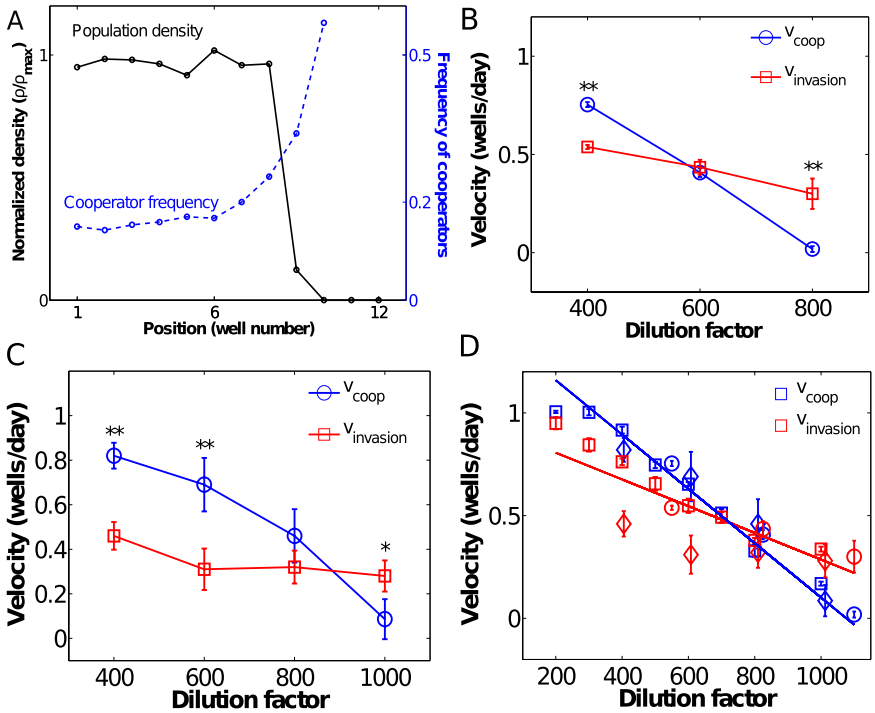

Fig. S8. Results are qualitatively reproducible across experiments. (*A*) An overlay of the density profile (in black) with the cooperator frequency profile (in blue) from d 9 of the expansion of a mixed cooperator–defector population (m = 0.5 and dilution factor = 400). The density profile is normalized to the maximum density found in the bulk population (ρ_{max}). Consistent with data shown in the main text, the cooperative allele is strongly enriched at the front of the expanding population. (*B*) Replicate measurements of the velocities of pure cooperators (v_{coop}) and invading defectors $(v_{invasion})$ over a range of dilution factors. Asterisks indicate the magnitude of the P value for the difference between v_{coop} and $v_{invasion}$ at a particular dilution factor (*$P < 0.05$, **$P < 0.01$, ***$P < 0.001$). Error bars for velocities are SEs in the slope of the X_m vs. time plot. (*C*) Additional replicate measurements of the velocities of pure cooperators (v_{coop}) and invading defectors $(v_{invasion})$ over a range of dilution factors. Asterisks are the same as in *B*. In all three experimental replicates (including that shown in the main text), we found that there were two regimes, where at high dilution factors defectors invade more quickly than the cooperators can escape $(v_{coop} < v_{invasion})$, and at low dilution factors, cooperators can "outrun" the invasion $(v_{coop} > v_{invasion})$. (*D*) A comparison of the velocity of expanding cooperators (v_{coop}) and the velocity of invading defectors $(v_{invasion})$ as a function of dilution factor. Data are compiled from three independent experiments. To account for experiment-to-experiment variability, all v_{coop} data were normalized by their x intercept (that is, the extrapolated dilution factor where $v_{coop} = 0$) (normalization factors were determined empirically to be 1.4 and 1.01 for data shown in *B* and *C*, respectively). Dilution factors for the corresponding invasion velocities were rescaled by the same factor. We then compared the slopes of v_{coop} and $v_{invasion}$ as a function of dilution factor by using a multiple linear regression model (analogous to that discussed in *SI Materials and Methods*). Although there is a great deal of variation between experiments, the crossing of v_{coop} and $v_{invasion}$ is still statistically significant $(p = 4 \times 10^{-4})$. We note that the exact correspondence between velocity and dilution factor was highly variable between experiments. In simulations, we found that this difference could be explained by a 2% decrease in the growth rates of the two strains, which could easily arise through small variations in the media formulation or growth conditions. As a result, experiment-to-experiment variation primarily captures small variations in media formulation, differences in the temperature of the incubator or the room on a given week, or intrinsic differences between single colonies.